Earth and Planetary Science Letters 300 (2010) 299–310

Contents lists available at ScienceDirect

Earth and Planetary Science Letters

journal homepage: www.elsevier.com/locate/epsl

The lithosphere–asthenosphere boundary and cratonic lithospheric layering beneath Australia from Sp wave imaging

Heather A. Ford [a,*], Karen M. Fischer [a], David L. Abt [a,1], Catherine A. Rychert [b,2], Linda T. Elkins-Tanton [c]

[a] Department of Geological Sciences, Brown University, Providence, RI, USA
[b] Institute of Geophysics and Planetary Physics, Scripps Institute of Oceanography, University of California, San Diego, CA, USA
[c] Department of Earth, Atmospheric and Planetary Sciences, Massachusetts Institute of Technology, Cambridge, MA, USA

ARTICLE INFO

Article history:
Received 27 May 2010
Received in revised form 4 October 2010
Accepted 5 October 2010
Available online 11 November 2010

Editor: T.M. Harrison

Keywords:
Australia
lithosphere
asthenosphere
receiver functions
magmatism

ABSTRACT

Sp and Ps scattered wave receiver functions were calculated for nineteen stations across Australia and the island of Tasmania in order to image the lithosphere–asthenosphere boundary and layering within the lithosphere. Within Phanerozoic eastern Australia and the eastern margin of the South Australia Craton, prominent Sp phases from a negative velocity contrast were found at depths of 61 ± 11 km to 131 ± 9 km, consistent with the lithosphere–asthenosphere boundary depth range from surface wave tomography. These phases imply significant velocity drops over depth ranges of 30–40 km or less, and thus cannot be explained by a lithosphere–asthenosphere boundary that is controlled by temperature alone. Rather, they imply that the asthenosphere is hydrated with respect to a drier, depleted lithosphere or contains a small amount of partial melt. The shallowest Sp phases have the largest amplitudes and occur in regions with the most recent, voluminous volcanism, strengthening the link to partial melt at the base of the lithosphere. In contrast, no significant negative Sp phases were found at the base of the thick cratonic lithosphere at the stations in central and western Australia, implying that the cratonic lithosphere–asthenosphere velocity gradient is distributed over more than 50–70 km in depth. This gradient may be purely thermal in origin, although gradational changes in composition or melt content cannot be ruled out. A negative Sp phase was observed at depths of 69 ± 8 km to 85 ± 14 km at stations in central and western Australia, indicating the presence of a drop in velocity internal to the lithosphere. This interface within the lithosphere may be a relic of cratonic mantle formation, or the result of alteration by melt and metasomatism.

1. Introduction

Although the lithosphere is commonly defined as the strong, thermally conducting outer shell of the earth, its physical and chemical properties, its formation and evolution, and the mechanism for its stability, are still poorly understood, particularly beneath continents. Insight on these issues may be gained by determining the depths of the lithosphere–asthenosphere boundary (LAB) and any discontinuities internal to the lithosphere, the seismic velocity gradients associated with these discontinuities, and their variation among tectonic provinces. In this study, we focus on the continental lithosphere of Australia.

1.1. Overview of Australian tectonics

The continent of Australia can be divided into three principal tectonic regions (Fig. 1), which include the predominantly Archean West Australia Craton, the largely Proterozoic North and South Australia Cratons in central Australia, and the Phanerozoic accreted terranes located in the eastern portion of the continent.

The West Australia Craton is the product of accretion of two Archean cratons, the Pilbara and Yilgarn, during the paleo-Proterozoic (Barley et al., 1998; Betts et al., 2002; Cawood and Tyler, 2004). The North Australia and South Australia Cratons, located in central Australia, are amalgamations of Archean and Proterozoic terranes that assembled during the Proterozoic (Betts et al., 2002; Giles et al., 2001; Tyler, 2001). A long-lived accretionary margin along the southern edge of the North Australia Craton resulted in collision with the West Australia Craton and with portions of the South Australia Craton during the paleo-Proterozoic (Betts et al., 2002).

During the Phanerozoic, accretion continued along the eastern margin of the Precambrian craton(s) in a series of subduction related events (Betts et al., 2002). The Tasman Line, first defined by the work of Hill (1951) through outcrop mapping, was thought to be a boundary

* Corresponding author. Department of Geological Sciences, Brown University, 324 Brook St. Box 1846, Providence, RI 02912, USA. Tel.: +1 401 863 1701; fax: +1 401 863 2058.
E-mail address: Heather_Ford@brown.edu (H.A. Ford).
[1] Present address: ExxonMobil Exploration Company, Houston, Texas, USA.
[2] Present address: Department of Earth Sciences, University of Bristol, Bristol, United Kingdom.

0012-821X/$ – see front matter © 2010 Elsevier B.V. All rights reserved.
doi:10.1016/j.epsl.2010.10.007

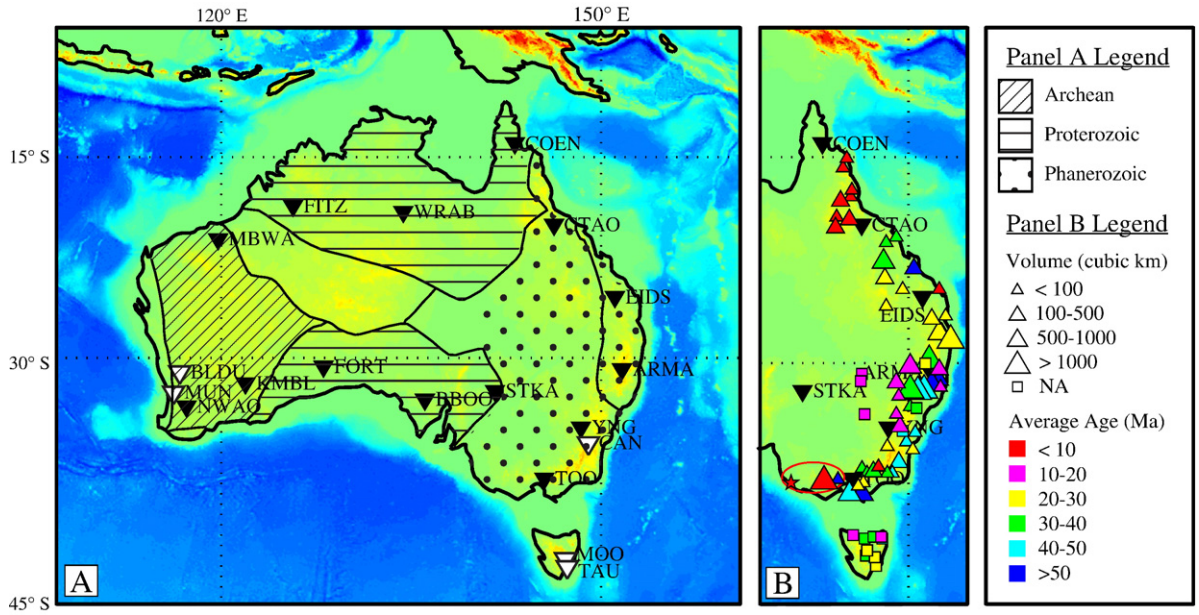

Fig. 1. (A) Overview of major tectonic provinces within Australia; solid black lines outline the seven major geophysical domains (Wellman, 1998). Region with inclined lines is the West Australia Craton (WC); horizontal lines indicate the North (NC) and South Australia (SC) Cratons; dots indicate the presence of Phanerozoic basement inferred from the Tasman Line (Gunn et al., 1997). The nineteen stations for which Ps and Sp receiver functions are calculated are marked with an inverted triangle. Black inverted triangles indicate the receiver functions are included in later interpretation. (B) Volcanism related to central and lava field volcanism (from Johnson et al., 1989). Volcanic age is indicated by color and volume is shown by size of the symbol. Star and oval show location of most recent volcanism.

dividing Proterozoic craton from Phanerozoic basement. However, more research has led to a number of different proposed locations and interpretations of the Tasman Line and a recent review has concluded that the accretion of eastern Australia onto the craton cannot be defined by a single line (Direen and Crawford, 2003). In addition to accretion, more recent Cenozoic volcanism (perhaps associated with mantle plumes (e.g. Wellman, 1983)) has impacted much of the eastern margin (Fig. 1). Magmatic ages from central volcanoes follow a well-established decrease from north to south, whereas lava field volcanism follows no known trend in age (Johnson et al., 1989; Wellman and McDougall, 1974). Over the last 10 My, the largest volumes of magmatism have occurred at the southern and northern reaches of eastern Australia (Fig. 1), with eruptions as recently as 4600 years ago within the Newer Volcanics in the south and 13,000 years ago in the north (Johnson et al., 1989).

1.2. Results from surface wave tomography

At the continental scale, surface wave tomography has indicated dramatically thicker lithosphere beneath cratonic Australia (150–250 km) than beneath Phanerozoic eastern Australia (as thin as 50 km) (Debayle and Kennett, 2000; Fichtner et al., 2009, 2010; Fishwick et al., 2005, 2008; Fishwick and Reading, 2008; Simons and van der Hilst, 2002, 2003; Simons et al., 1999). However, more detailed estimates of lithospheric thickness and its correlation with crustal age differ between these studies. Although surface wave tomography is excellent for imaging volumetric heterogeneity, it cannot distinguish between differences in vertical mantle velocity gradient thicknesses that occur over depth ranges of 50 km or less. S-to-P (Sp) and P-to-S (Ps) scattered waves are a good alternative for studying the nature of the LAB and other mantle interfaces because of their ability to more precisely constrain boundary depths and vertical velocity gradients.

The LAB has been inferred in a variety of tectonic settings from Ps receiver functions (e.g., Chen et al., 2006; Collins et al., 2002; Li et al., 2000; Ozacar et al., 2008; Rychert and Shearer, 2009; Rychert et al., 2005; Snyder, 2008; Wolbern et al., 2006) and Sp receiver functions (e.g., Abt et al., 2010; Hansen et al., 2007, 2009; Heit et al., 2007; Kumar et al., 2005a,b, 2007; Li et al., 2004, 2007; Mohsen et al., 2006; Oreshin et al., 2002; Sacks et al., 1979; Sodoudi et al., 2006; Vinnik et al., 2005) or a combination of both (e.g. Kawakatsu et al., 2009; Rychert et al., 2007; Wittlinger and Farra, 2007). Reviews may be found in Fischer et al. (2010) and Rychert et al. (2010). In Australia, a number of studies using Ps receiver functions have imaged the seismic crust–mantle boundary (Moho) (e.g. Clitheroe et al., 2000a,b; Reading and Kennett, 2003; Reading et al., 2003, 2007). A Sp receiver function study by Kumar et al. (2007) observed a negative phase at four stations in Australia and interpreted it as the LAB at depths ranging from 90 km to 207 km. In contrast, a Ps study by Rychert and Shearer (2009) identified a negative phase at five stations at depths of 71–106 km and interpreted it as the LAB off the craton or a mid-lithospheric discontinuity within the craton. Our study more completely characterizes the LAB and mid-lithospheric discontinuities throughout Australia with Sp receiver functions that sample all three primary tectonic regions.

2. Method

2.1. Ps and Sp receiver functions

The basic premise of the receiver function method is that the deconvolution of the parent phase (e.g., P for Ps; SV for Sp) from the daughter component (e.g., SV for Ps; P for Sp) removes source and instrument effects, enhancing information regarding seismic structure beneath the station of interest. Although Ps receiver function analysis has been successfully used for many years to image the Moho and relatively deep mantle discontinuities such as those in the transition zone, interpretation of phases in terms of shallow upper mantle structure requires great care due to the presence of crustal multiples which can contaminate direct arrivals; these effects are typically most pronounced at depths of less than 200–250 km (e.g. Bostock, 1998; Rychert et al., 2005, 2007). In Sp receiver functions, reverberations associated with the crust arrive after the direct S phase, while scattered Sp phases arrive before the direct phase. This separation prevents contamination by crustal multiples, making Sp scattered waves a useful tool for imaging upper mantle discontinuities

such as the lithosphere–asthenosphere boundary. Limitations of Sp phases include possible interference with SKS and SKSp at distances greater than 75° and with P-wave phases, such as pPPP, pPPPP, and sPPPP, for events at depths greater than 300 km (Wilson et al., 2006), and the fact that they are not produced at mantle depths for distances of less than roughly 55° (Yuan et al., 2006). In addition, Ps waves are often better at resolving the depth extent of vertical velocity gradients that are distributed over less than 20–30 km, due to their higher frequency energy content. Moreover, because the paths of incoming Ps phases are closer to vertical than Sp paths for a given source–station distance, they sample a smaller region around the station, reducing the potential for averaging of laterally-varying discontinuity structure.

As a result of the above considerations both Ps and Sp were analyzed, with distance limits of 35°–80° for Ps and 55°–75° for Sp (Fig. 2), and a depth limit of less than 300 km for Sp. Receiver functions were binned by epicentral distance in order to differentiate phases of interest from crustal multiples in Ps and unwanted teleseismic phases in Sp.

2.2. Data preparation

Receiver functions were calculated for nineteen permanent broadband stations located in Australia and on the island of Tasmania. An event list was compiled from the USGS National Earthquake Information Center (NEIC) global event catalog and included events with an $M_w \geq 5.8$, an epicentral distance of 35°–80° and no restrictions in depth, occurring through March 2009. Waveform data was obtained from the Incorporated Research Institutions for Seismology (IRIS) Data Management Center (DMC) and included data from networks AU, G, II and IU. The number of waveforms used varies between stations due to differences in quality as well as station operation time (Table 1). A free surface transfer matrix (Bostock, 1998; Kennett, 1991) was used to transform the recorded waveforms into the P and SV components that would have been incident on the free surface, assuming a given ray parameter and surface Vp and Vs. To optimize the free surface transformation, the surface Vp and Vs for each station were determined using an automated procedure that is detailed in Abt et al. (2010). Essentially, the parent phase on each waveform (P for Ps or SV for Sp) was windowed around its arrival time, and a search was performed over a range of Vp and Vp/Vs to find the value(s) that minimized the correlation of the parent phase with its corresponding window on the daughter component (SV for Ps and P for Sp). For each station, all cross-correlation surfaces with well-defined minima were stacked, and the best free surface velocities for the station were defined as the minimum of this stack. During this process, checks were put into place to ensure that only quality waveforms were included in the analysis. These measures included rejecting waveforms with signal-to-noise ratios below a selected value (5 for Ps and 2 for Sp) and whose observed arrival-times differed from the predictions of the AK135 velocity model (Kennett et al., 1995) by more than 5 s for Ps or 10 s for Sp.

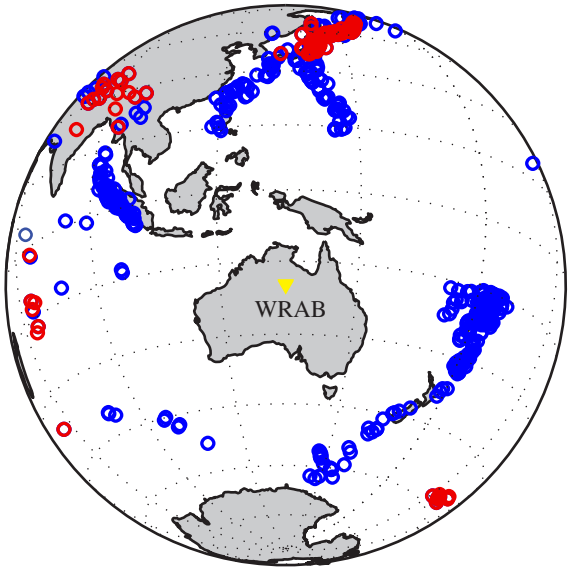

Fig. 2. Distribution of events used to calculate Ps (blue circles) and Sp (red circles) receiver functions for station WRAB. A total of 523 events from epicentral distances of 35°–80° were used for Ps at WRAB and 121 events from epicentral distances of 55°–75° were used for Sp at WRAB.

2.3. Deconvolution and migration

We employed two different deconvolution techniques in order to ensure that phases observed on the receiver functions were not artifacts of a given deconvolution approach. In the first method, all waveforms for a given phase (Sp or Ps) and station were simultaneously deconvolved and migrated in the frequency domain, using a best fitting regularization parameter (i.e. water-level) to stabilize the deconvolution (Bostock, 1998). In the second approach, iterative time-domain deconvolution (Kikuchi and Kanamori, 1982; Ligorria and Ammon, 1999) was applied to individual Sp or Ps and waveforms; waveforms for a given phase (Sp or Ps) and station were then migrated and stacked. Prior to deconvolution the waveforms are bandpass filtered (0.03–1 for Ps and 0.03–0.5 for Sp). The 1-D velocity models used for migration vary between stations. Crustal thickness and Vp and Vs values were obtained from H-k stacking (Zhu and Kanamori, 2000) of Ps waveforms. H-k stacking results were considered robust if the estimated Moho depth fell within the error bars of the Moho phase selected from the Ps receiver function. Complicated crustal structure at FORT, where H-k stacking was unable to constrain a single best pick, required a fixed crustal model constructed using estimates of Moho depth from Clitheroe et al. (2000a). AK135 (Kennett et al., 1995) was assumed for the mantle at all stations. This choice of 1D mantle velocity model does not account for possible variations in mantle Vp/Vs and may produce systematic errors in phase depth estimation. We estimate that the resulting uncertainty in inferred mantle discontinuity depths is on the order of 10 km or less. For example, Rychert et al. (2007) demonstrated that changing Vp/Vs from 1.7 to 1.8 could vary the depth of a phase located at approximately 90 km in a Sp receiver function by roughly 6–8 km. Abt et al. (2010) migrated Sp and Ps data using two different mantle velocity models, AK135 and 1D profiles extracted from 3D Vs (Yuan and Romanowicz, 2010) and Vp (Burdick et al., 2008) models for North America, and found that differences in inferred discontinuity depths in the 50 to 115 km range were 6 km or less. Kaiho and Kennett (2000) observed as much as a 6% Vp/Vs decrease with respect to AK135 in parts of northern Australia at depths of 35–120 km. If a 6% Vp/Vs drop is assumed, Sp phases that would appear at 130 km in an AK135 mantle would instead be located at 140 km. A discontinuity at a depth of ~75 km would only be perturbed by 5 km.

For a given depth in the migration, a waveform was included only if a direct, pre-critical phase was predicted to exist for the direct phase ray parameter, assuming the 1D velocity model for the given station. This step reduces the number of events at a given depth in addition to eliminating deeper portions of some Sp receiver functions. For example, at a depth of 380 km only events with a ray parameter of 0.105 (70° epicentral distance) or smaller are included, whereas at a depth of 150 km, the largest ray parameter that can be included is 0.120 (55° epicentral distance). Ps phases do not reach post-critical

Table 1
Summary of receiver function results at the eighteen stations used in the study. The velocity model used for the migration for all but FORT was created using a crustal model from Ps H-k stacking for the respective station and a mantle model from AK135. The Moho phase depths listed in the table were obtained from Ps receiver functions, except for FORT* which was obtained from the Sp receiver function. The largest statistically significant negative phase for each station was selected from Sp receiver functions. Phase depth uncertainties correspond to the maximum range of depth in between where the bootstrap two standard deviations have the same amplitude as the phase peak of the bootstrap mean. A negative phase is not listed for stations where the time-domain and frequency-domain deconvolution methods yielded significantly different receiver function results. The potential "LAB depth range" was determined from the updated shear wave velocity model (Fishwick et al., 2008) and corresponds to the depth range between the minimum Vs beneath the Moho up to the next local maximum in velocity. Stations where there is no high velocity lid present beneath 75 km are designated with the label "Absent Lid" and the LAB depth range is assumed to be between the Moho and 75 km. If the negative phase pick from the Sp receiver functions falls within the LAB depth range, the phase is interpreted as the LAB otherwise it is interpreted to be a mid-lithospheric discontinuity (MLD). BBOO is the one exception. See Section 3 for a more detailed discussion.

		Events		Crustal velocity model				Phases and interpretation			
Net	STA	#Ps	#Sp	Model	Moho	Vp	Vp/Vs	Moho	Negative Phase	LAB depth range	Boundary
AU	ARMA	199	112	H-k stack	34	6.42	1.72	36 ± 3	93 ± 16	<150 km	LAB
AU	BBOO	192	58	H-k stack	41	6.55	1.77	42 ± 3	131 ± 9	150–175 km	LAB
AU	BLDU	13	2	H-k stack	35	6.42	1.73	36 ± 2	–	–	–
AU	COEN	266	70	H-k stack	37	6.47	1.7	38 ± 2	67 ± 8	Absent Lid	LAB
AU	EIDS	209	112	H-k stack	35	6.51	1.7	37 ± 3	76 ± 12	<150 km	LAB
AU	FITZ	279	59	H-k stack	41	6.45	1.71	44 ± 5	81 ± 8	125–225 km	MLD
AU	FORT	169	44	Fixed	40	6.45	1.85	40 ± 9*	79 ± 6	125–200 km	MLD
AU	KMBL	294	64	H-k stack	37	6.46	1.73	38 ± 1	85 ± 14	125–225 km	MLD
AU	MOO	84	39	H-k stack	33	6.27	1.68	33 ± 3	–	–	–
AU	MUN	151	34	H-k stack	51	6.42	1.87	53 ± 2	–	–	–
AU	STKA	333	97	H-k stack	43	6.47	1.68	46 ± 3	104 ± 9	100–175 km	LAB
AU	TOO	216	91	H-k stack	33	6.43	1.77	34 ± 3	61 ± 11	Absent Lid	LAB
AU	YNG	184	79	H-k stack	34	6.57	1.83	33 ± 2	70 ± 8	<150 km	LAB
II	TAU	313	120	H-k stack	31	6.18	1.74	32 ± 3	–	–	–
II	WRAB	523	121	H-k stack	48	6.58	1.74	49 ± 2	81 ± 14	175–200 km	MLD
IU	CTAO	619	251	H-k stack	39	6.51	1.7	40 ± 2	73 ± 6	Absent Lid	LAB
IU	MBWA	349	129	H-k stack	31	6.51	1.69	32 ± 2	69 ± 8	100–200 km	MLD
IU	NWAO	372	176	H-k stack	38	6.46	1.78	41 ± 3	81 ± 8	100–175 km	MLD

incidence over the range of epicentral distances and depths included in this study.

In order to understand the uncertainties associated with each receiver function, error bars were calculated using a bootstrap test in which 20% of the waveforms were randomly replaced with another random 20%. The replacement and recalculation was repeated 100 times in order to determine the mean and standard deviation.

3. Results

Ps and Sp receiver functions were calculated for the nineteen stations shown in Figure 1 using the frequency- and time-domain deconvolution techniques. At fourteen stations, these methods produced consistent Sp and Ps receiver functions. For example, at station ARMA (Fig. 3) the depth to the large, positive (Moho) phase is very similar on the Sp receiver functions generated by the different deconvolution methods. Moreover, the largest negative phase present on the frequency-domain receiver function is found at a depth of 93 ± 16 km while the largest negative phase on the time-domain receiver function is found at a depth of 81 ± 18 km; each estimate is within the error bars of the other. Receiver functions that varied greatly between the time- and frequency-domain (e.g. negative phases not within error of each other) were discarded, whereas stations where the two methods yielded receiver functions with comparable shape and phase depths were included in the interpretation. Moho and upper mantle discontinuity depths measured from the frequency-domain receiver functions are listed in Table 1.

For each station, Moho depth was found from the largest positive phase on the single-binned Ps receiver function. Measured Moho depths were in general consistent between Ps and Sp receiver functions and agree with crustal thickness estimates from H-k stacking where the latter exist (Table 1). In Phanerozoic Australia, Moho depths range from 32 ± 2 km at TAU to 40 ± 2 km at CTAO. On the craton, Moho depths vary from 32 ± 2 km at MBWA to 53 ± 2 km at MUN.

Phases associated with upper mantle discontinuities were interpreted from Sp receiver functions. Most of the Ps receiver functions also contain negative energy at depths similar to the negative phases seen in Sp receiver functions. However, strong reverberations in Ps receiver functions, including apparent reverberations from intracrustral layering that exhibit negligible moveout with epicentral distance, complicate the interpretation of possible upper mantle discontinuities, leading us to report and interpret mantle phases only from Sp receiver functions. At station TOO both Ps and Sp receiver functions have strong, well-resolved negative phases (Fig. 4a and b) found within error of each other. It is possible that the negative phase in Ps is the result of an upper mantle discontinuity; however, influence from a midcrustal discontinuity cannot be ruled out. At station FORT the presence of shallow crustal layering produces reverberations that could potentially interfere with upper mantle phases within the Ps receiver function (Fig. 4c). The strong negative arrival observed at 79 ± 6 km on the Sp receiver function for FORT does not suffer from reverberation contamination (Fig. 4d).

At mantle depths, Sp receiver functions are in general dominated by a single negative phase over the depth range imaged. We interpret this phase and report its depth in Table 1 when it is reasonably consistent across epicentral distance bins at a given station (e.g. Fig. 5) and between frequency- and time-domain deconvolution results. Although smaller arrivals also appear in the Sp receiver functions, they are less consistent between stations and often also less consistent as a function of epicentral distance. In order to determine whether our negative phase pick from the Sp receiver function is the LAB or some other upper mantle discontinuity we compared the depth of our pick for a given station to the corresponding absolute shear wave velocity profile (from 75 to 300 kilometers) constructed from the updated shear wave velocity model of Fishwick et al. (2008). For the negative phase pick of the Sp receiver function to be interpreted as the LAB, it must fall within the depth range between the minimum Vs beneath the Moho (which presumably lies within the asthenosphere) and the next maximum in Vs in the upward direction (which presumably lies within the lithosphere). At three stations in eastern Australia (COEN, CTAO, and TOO) the minimum Vs lies at 75 km, which corresponds to the top of the Fishwick

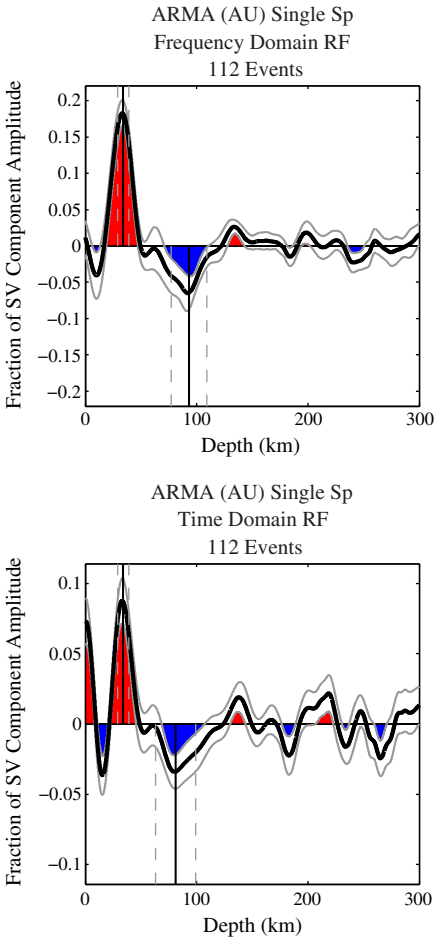

Fig. 3. Comparison of single-binned Sp receiver functions for station ARMA calculated using frequency-domain (a) and time-domain (b) deconvolution methods. The thick, solid black line is the mean calculated receiver function from the bootstrap test. The mean is virtually identical to the single-stacked receiver function. The solid grey lines on either side of the mean are the two standard deviations. The receiver functions are similar in form, with a strong positive phase at a depth of 34 ± 5 km in the frequency domain and 33 ± 5 km in the time domain, which is interpreted as the Moho. At 93 ± 16 km (a) and 81 ± 18 km (b) a robust negative phase corresponds to the estimated LAB depth from the shear wave velocity model of Fishwick et al. (2008). A phase is only considered robust if there is good agreement between the time and frequency domains.

et al. (2008) model; in these cases the potential LAB depth range is assumed to be from the Moho to 75 km. If the depth of the negative phase is above the LAB depth range, then it is considered to be a mid-lithospheric discontinuity (MLD). Station BBOO is the one exception, as discussed in Section 3.2.

3.1. Phanerozoic Australia

Of the nine stations within Phanerozoic Australia, six were found to have consistent Sp receiver functions from time- and frequency-domain deconvolution methods (e.g. station ARMA, Fig. 3). In regard to the other three, at MOO and TAU constraints on Moho depth were obtained from Ps receiver functions and H-k stacking (Table 1); at CAN, even crustal structure was not well constrained. Station COEN (Fig. 5) is representative of other stations located along the eastern margin of the continent. The Sp receiver function contains a strong negative phase at 67 ± 8 km that lies within the potential LAB depth range and is interpreted as the lithosphere–asthenosphere boundary.

Sp receiver functions for the six Phanerozoic stations show well-resolved negative phases that range in depth from 61 ± 11 km at TOO to 93 ± 16 km at ARMA (Fig. 6b and Table 1). All of these phases fall within the potential LAB depth range defined from the shear wave model of Fishwick et al. (2008) and are interpreted as the LAB.

3.2. Cratonic Australia

Within the Proterozoic and Archean portions of the Australian continent, Ps and Sp receiver functions were calculated for ten stations. Of these stations eight have interpretable mantle Sp phases, while at BLDU and MUN only crustral structure was obtained. Figure 6c and d shows two profiles of the Sp receiver functions in southern and northern Australia that intersect Archean, Proterozoic and Phanerozoic terranes.

Stations STKA and BBOO are located near the eastern edge of cratonic Australia (Fig. 1). At STKA, the largest significant negative phase in Sp is located at a depth of 104 ± 9 km and is consistent between bins of epicentral distance (Fig. 5). The negative phase falls within, but near the edge of, the potential LAB depth range for the absolute Vs profile beneath STKA and is interpreted to be the LAB (Fig. 6c). To the west of STKA, station BBOO's deepest, most statistically significant negative phase is found at 131 ± 9 km (Fig. 6c). This depth falls outside of the potential LAB depth range estimated from the Vs profile and the phase could be interpreted to represent a mid-lithospheric discontinuity (MLD). However, the negative phase lies only 10 km outside of potential LAB depth range. In addition, its depth is considerably greater than the MLD phases observed at other cratonic stations. Thus we interpret the negative phase to be the LAB, while acknowledging the ambiguity of this choice. If the negative phases at STKA and BBOO are interpreted to be LAB, then an argument could be made for a dipping boundary that increases in depth to the west (Fig. 6c).

At the remaining stations within cratonic Australia, a prominent negative Sp phase is observed within the cratonic lithosphere (a MLD), but no clear arrival is observed from depths comparable to the LAB (Fig. 6c and d). Station WRAB is located well within the interior of the North Australia Craton. A large negative phase at a depth of 81 ± 14 km appears in the single-binned receiver function and is also consistent between bins of epicentral distance (Fig. 5). The inferred LAB depth range at WRAB from Fishwick et al. (2008) is 175–200 km, which is significantly deeper than the largest negative phase on the Sp receiver function, leading to the latter's interpretation as a MLD. No significant negative phase occurs in the LAB depth range at WRAB. Elsewhere in the craton along the northern profile (Fig. 6d), the largest negative phases at FITZ and MBWA are similar in depth to the negative phase at WRAB. They also lie above the potential LAB depth range and each is inferred to be a MLD. Along the southern margin of the craton at stations FORT, KMBL, and NWAO (Fig. 6c) the negative Sp phase depths are too shallow to be the LAB when compared to the respective shear wave velocity profile and are each taken to be a MLD. No significant negative phase occurs within the LAB depth range at these stations.

It should also be noted that although the receiver functions are displayed to depths of 250 km, both Ps and Sp receiver functions were calculated to 400 km for all stations and were examined to determine whether significant, well-constrained phases existed at greater depths. In Sp receiver functions, depths greater than approximately 250–300 km are often noisy and poorly constrained, with large differences in time and frequency-domain deconvolution methods. This is due to the small number of waveforms included as a result of our removing waveforms from depths for which no direct, pre-critical phase was predicted to exist. Although we cannot rule out the possibility of a significant negative Sp phase at depths of 250–400 km, such an arrival would lie well below the potential LAB depth range from the Fishwick et al. (2008) velocity model.

3.3. Large-scale correlation in depth and amplitude estimates

In order to better visualize how the LAB and MLD vary between stations, two plots of smoothed Sp conversion points, color-coded as a

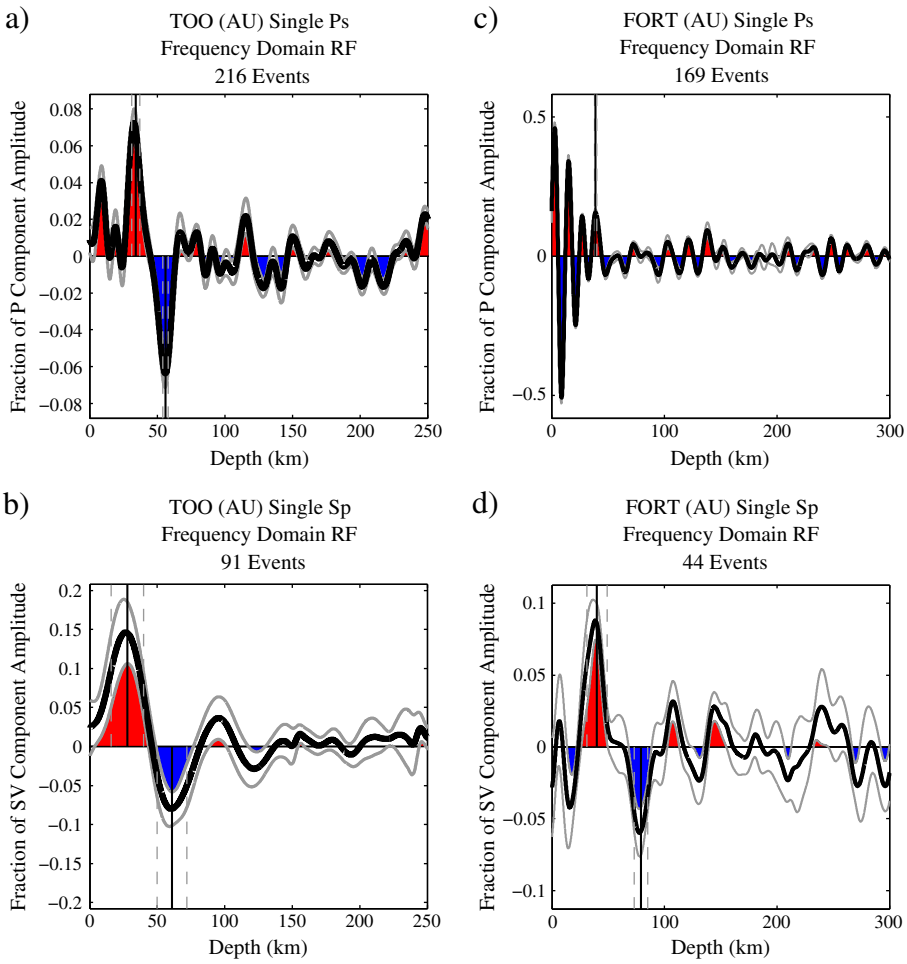

Fig. 4. Example of single bin Ps and Sp receiver functions calculated for stations TOO (a and b) and FORT (c and d). The Ps receiver function for TOO (a) exhibits a strong, well-defined positive phase at 34 ± 3 km indicating a velocity increase with depth, interpreted as the Moho. A negative phase is observed at 56 ± 2 km and is consistent with the negative phase in Sp (b) at a depth of 61 ± 11 km. The Ps receiver function at FORT (c) has complicated crustal structure with numerous reverberations, in contrast to the Sp receiver function at FORT (d), which exhibits a clear signal, with a strong negative phase indicating a velocity decrease with depth at 79 ± 6 km. This negative phase is not apparent on the Ps receiver function (c), which may be due to interference from reverberations.

function of depth and amplitude, are shown in Figure 7 (see figure caption for smoothing details). From this point forward, stations whose negative phase is interpreted to be the LAB will be referred to as stations of eastern Australia. It should be noted that these stations sample mantle beneath both cratonic (STKA and BBOO) and Phanerozoic (COEN, CTAO, EIDS, ARMA, YNG, TOO) regions. Stations that are referred to as being located in central and western Australia are cratonic stations and have a negative phase interpreted to be a MLD.

In eastern Australia, a large variation occurs in the depth and amplitude of the LAB phase (Fig. 7), and depth and amplitude are negatively correlated. Where the LAB is found to be relatively shallow, its amplitude is larger (Fig. 8). Intriguingly, the locations of the shallowest, strongest amplitude, negative phases fall in or near regions of the most recent, voluminous volcanism (see Fig. 1). The relationship between these observations is further discussed in Section 4.3. In contrast, the depths and amplitudes of the MLD phases observed in central and western Australia are more tightly clustered (Fig. 8) and no observable variation exists between cratonic blocks.

4. Discussion

4.1. Comparison to other receiver function studies

Previous receiver function studies in Australia have used Ps scattered waves to determine crustal structure (Clitheroe et al., 2000a,b; Reading and Kennett, 2003; Reading et al., 2003, 2007). A continent-wide study of crustal structure by Clitheroe et al. (2000a) found crustal thickness values at/near several stations in our study, including CTAO, ARMA, KMBL, NWAO, and WRAB (see Fig. 8 Clitheroe et al., 2000a,b). At these locations the Moho depth from our results and the results of Clitheroe et al. (2000a) are within error of each other. More recent work by Reading et al. (2003) found that the crustal thickness of the Yilgarn Craton varies slightly from west to east, but is approximately 35 to 40 km, which agrees well with our results at stations NWAO and KMBL. Reading and Kennett (2003) found that Moho depth is 30 ± 2 km in the Pilbara Craton, in agreement with our measured Moho depth of 32 ± 2 km at station MBWA.

Turning to the mantle, a Sp receiver function study by Kumar et al. (2007) interpreted the depth of the LAB at stations NWAO, WRAB, and STKA to be 164 km, 180 km, and 207 km respectively. In contrast, we did not find any significant negative phase at these depths at NWAO and WRAB. At STKA, a small amount of negative energy does appear around 200 km, but its amplitude is much smaller than the phase we observe at 104 ± 9 km. Our results are more consistent with the conclusions of Rychert and Shearer (2009) based on Ps receiver functions. Rychert and Shearer (2009) found discontinuity depths of 71 to 106 km for three of the same stations as our study, both on and off the craton. At NWAO they observe a negative phase at 71 km, which comes close to the negative phase at 81 ± 8 km observed from our Sp receiver function. At stations WRAB and CTAO, Rychert and

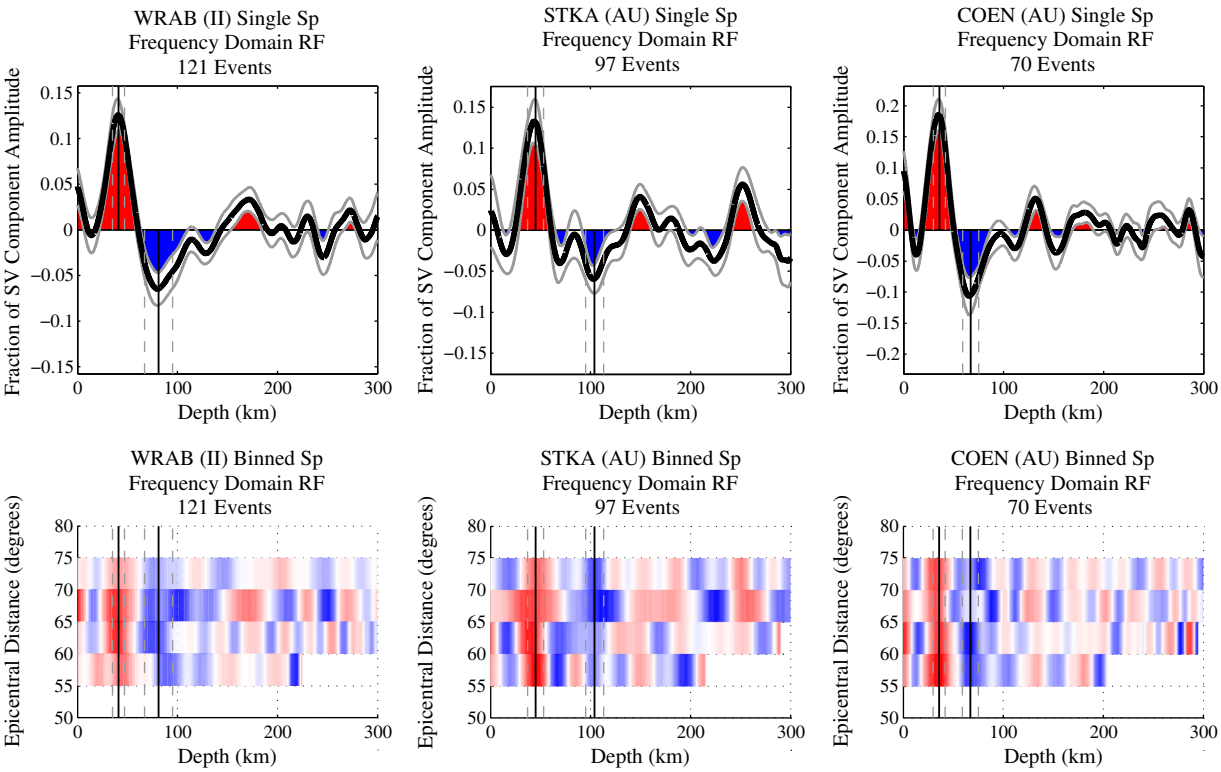

Fig. 5. Example of Sp receiver functions for three tectonically distinct regions. The thick, solid black line is the mean calculated receiver function from bootstrapping, where the solid grey lines on either side of the mean are the two standard deviations. (a–b) WRAB is located well within the interior of the Proterozoic North Australia Craton and is characterized by a negative phase at 81 ± 14 km that is interpreted to be mid-lithospheric discontinuity. (c–d) STKA is found along the ambiguously defined Proterozoic margin. The Sp receiver function is characterized by a well-constrained negative phase at 104 ± 9 km inferred to be the LAB. (e–f) The results at station COEN are typical of many receiver functions for stations along the eastern margin of the continent. A negative at 67 ± 8 km is interpreted to be the LAB.

Shearer (2009) identified negative phases at 106 and 86 km, respectively, which are 11 and 9 km outside of the error bars for the Sp arrivals we observe at those stations.

4.2. Estimating the gradient thickness and velocity contrast at a boundary

To better understand the mechanism(s) that may responsible for producing a boundary in seismic velocity, it is important to constrain the velocity gradient parameters that describe the boundary. In the case of the negative Sp phases considered in this study, the parameters are the velocity drop and the gradient thickness (the depth range over which the velocity drop is distributed). To more completely constrain the gradient parameters, detailed inverse modeling is needed (e.g., Rychert et al., 2005, 2007). However, simple forward modeling can still be useful in constraining the gradient and in differentiating between possible mechanisms.

For each modeled receiver function, velocity gradient parameters were systematically varied to determine the parameter ranges that provide acceptable fits to the observed LAB or MLD. The tested velocity models contained the specific crustal structure for the given station and an LAB or MLD described by velocity drop and gradient thickness values. Gradient thicknesses of 0 km to 90 km were tested at 10 km increments. Velocity decreases of up to 10% were considered; 10% is greater than the total shear velocity drop from lithosphere to asthenosphere typically seen in surface wave models (Gaherty et al., 1999; Nettles and Dziewonski, 2008; Romanowicz, 2009; Yuan and Romanowicz, 2010). A propagator matrix method (Keith and Crampin, 1977) was used to generate synthetic waveforms that were turned into receiver functions using the same processes that were applied to the observed seismograms. In the data, the dominant period of the incident S waveform was 10–11 s, and a source-time function with a dominant period of 10.5 s was employed in the synthetics. In addition, the number and distribution of ray parameters in the synthetic seismograms duplicated the distribution of events in the observed receiver functions. The results of the modeling are discussed in Sections 4.3, 4.4, and 4.5.

4.3. The lithosphere–asthenosphere boundary in eastern Australia

The negative Sp phase observed at depths of approximately 61 ± 11 km to 131 ± 9 km beneath stations in eastern Australia is interpreted to be the LAB based on comparison with shear wave velocity structure (Fishwick et al., 2008). To constrain the velocity gradient associated with the LAB, the LAB Sp phases were modeled for station COEN which has the largest amplitude LAB phase, ARMA which has the smallest amplitude LAB phase on the eastern margin of Australia, and BBOO which has the smallest amplitude LAB phase overall.

For station COEN, the best fitting velocity gradients vary from a 7% velocity decrease over 0 km, to a 10% decrease in velocity over 20 km (Fig. 9), but all models with gradient thicknesses of 40 km or more or velocity drops of 4% or less failed to match the observed receiver function to within two standard deviations. At station ARMA, the best fitting gradients vary from a 4% velocity drop over 0 km, to a 7% velocity drop over 10 km and a 10% drop in velocity over 20–30 km (Fig. 9). At ARMA and BBOO, a gradient thickness of 40 km for a 10% velocity drop grazes the lower amplitude two standard deviation limit of the observed Sp phases. Overall, for stations representing the range of LAB Sp phase amplitudes in eastern Australia, gradient thicknesses of 40 km or less are required, and smaller gradient thicknesses provide better fits.

In geodynamical models for cratonic lithosphere and surrounding continental margins (Cooper et al., 2004; King and Ritsema, 2000; Korenaga and Jordan, 2002) temperature gradients between the lithosphere and asthenosphere occur over at least 50–70 km. In contrast,

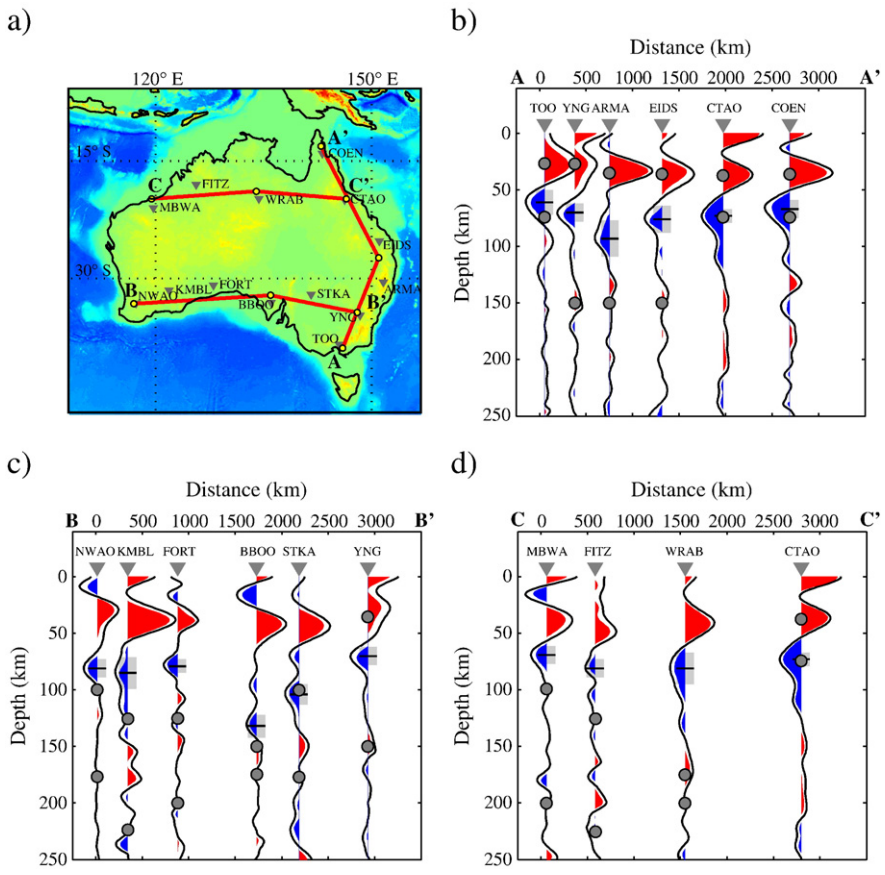

Fig. 6. (a) Lines demonstrating location of cross-sections of Sp receiver functions A–A′, B–B′ and C–C′. (b thru d) The mean of the bootstrapped receiver functions are shown in solid black in cross-sections A–A′, B–B′ and C–C′. The receiver functions are plotted to the same scale in each cross-section and the statistically significant portions are represented in either red (positive) or blue (negative). Depths are shown to 250 km, but individual receiver functions were examined to 400 km to ensure that no identifiable phases existed at greater depths. Black horizontal lines mark the location of the largest significant negative phase, and the surrounding grey box indicates the two standard deviations. Solid grey and black circles indicate the range of potential LAB depths from surface wave tomography (Fishwick et al., 2008). If the negative phase from the receiver function falls within the potential LAB depth range, the phase is interpreted to be the LAB; otherwise it is characterized as a MLD.

the modeling of eastern Australia LAB Sp phases in this study rules out velocity gradient thicknesses of more than 40 km. We thus conclude that the LAB in eastern Australia cannot be the result of a change in temperature alone.

Another possible explanation for the velocity drop is that the lithosphere is more dehydrated and depleted relative to a hydrated and fertile asthenosphere (Hirth and Kohlstedt, 1996; Karato and Jung, 1998). Mg numbers for the mantle of the Phanerozoic Australia lithosphere lie in the range of 90–91 (Gaul et al., 2000), relatively close to values expected for the asthenosphere (88–89), with the result that depletion alone could reduce velocities by less than 1% (Lee, 2003). However, hydration in the asthenosphere could create a drop in velocity of roughly 4.5% across the LAB (Rychert and Shearer, 2009), and thus could explain the eastern Australia LAB Sp phases, with or without depletion effects, assuming that the velocity gradient occurs over 10 km or less.

Alternatively, a small fraction of melt in the asthenosphere could produce a large drop in velocity. The exact percent melt needed to produce a given percent change in seismic wave speed depends on melt geometry (e.g., Hammond and Humphreys, 2000; Takei, 2002; Takei and Holtzman, 2009), but 1–2% appears to be sufficient (Hammond and Humphreys, 2000; Kawakatsu et al., 2009). The xenolith-based southeast Australia (SEA) geotherm (O'Reilly et al., 1997) is thought to reflect the present-day geotherm in high heat flow areas like north Queensland (e.g., COEN), east-central Queensland (e.g., CTAO) and western Victoria (e.g., TOO) (O'Reilly et al., 1997). O'Reilly et al. (1997) inferred that the SEA geotherm crossed the dry peridotite solidus at a depth of approximately 120 ± 20 km, significantly deeper than the negative velocity gradient indicated by the Sp phases. However, reduction of the asthenospheric solidus temperature due to hydration (e.g. Grove et al., 2006; Hirschmann et al., 2009) creates the possibility that the eastern Australia LAB coincides with the damp solidus and that the LAB velocity gradient reflects partial melt within the asthenosphere. Alternatively, small degrees of carbonatite melt may exist in the asthenosphere (Dasgupta and Hirschmann, 2007).

A link appears to exist between eastern Australia LAB properties, lithospheric temperature, and present-day partial melt. The highest heat flow areas (O'Reilly et al., 1997) coincide with regions of recent and voluminous volcanism (Fig. 1) and with stations COEN, CTAO, and TOO, where the lithosphere appears to be thinner and the amplitude of the LAB phase is larger than at other eastern Australia stations (Fig. 7). An interesting question is whether the zones of thinner lithosphere created (e.g., Ebinger and Sleep, 1998), or were created by, focused mantle flow and melting.

4.4. The lithosphere–asthenosphere boundary in central and western Australia

In the craton, surface wave tomography models indicate that the transition from seismically fast lithosphere to slow mantle asthenosphere occurs at depths of approximately 150–250 km in Australia (Fishwick et al., 2008). The absence of significant negative energy in

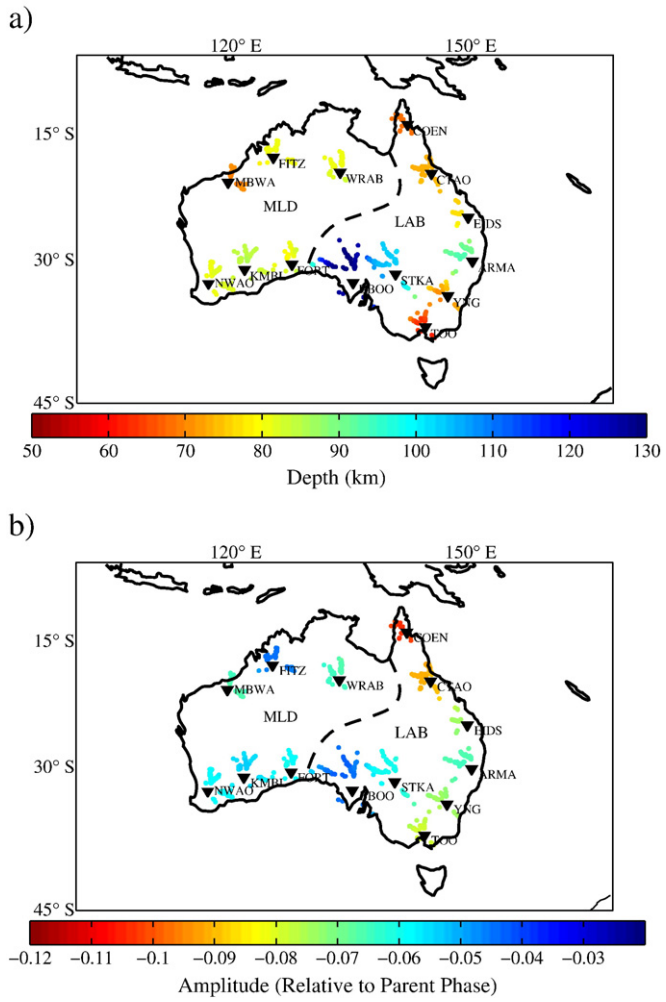

Fig. 7. Smoothed conversion depths (a) and amplitudes (b) of selected negative Sp phases. Negative phases are selected based on the largest, statistically significant negative peak within a given receiver function. The smoothed conversion point locations are created by first calculating the theoretical piercing points of the selected negative phase for each station using the respective H-k stacking crustal model combined with AK135 (Kennett et al., 1995) for the mantle. The piercing points were then placed onto a 0.05°×0.05° grid and were averaged if more than one piercing point fell onto a single element. The piercing points were then smoothed with a circular filter, which produced a new spacing of 0.3°. Upside-down black triangles indicate seismic station location. The thick dashed black line is used to graphically illustrate the separation between stations imaging the LAB and stations imaging a (MLD).

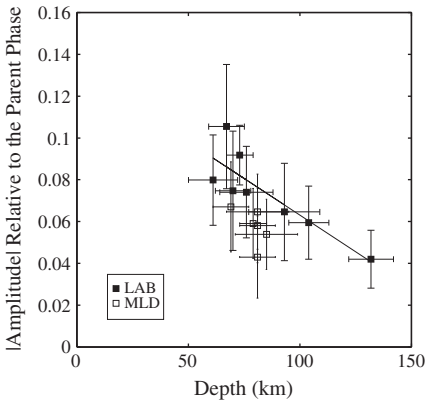

Fig. 8. Plot of amplitude versus depth of the negative phase interpreted to be the LAB (solid black squares) and the MLD (black and white squares) shown with two standard deviation error bars. Black line shows the best fit through the LAB phases.

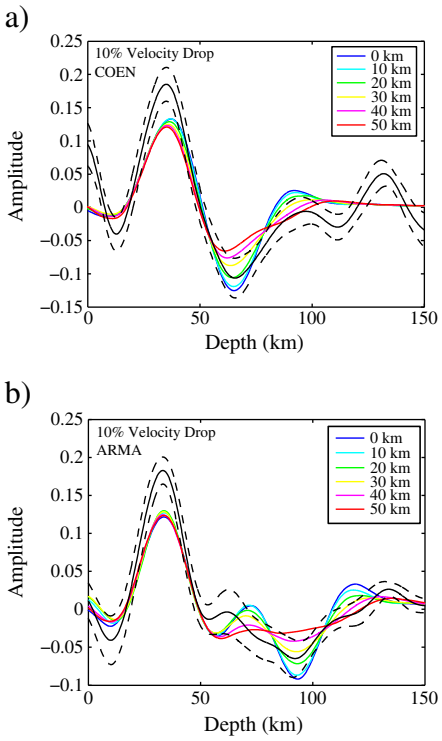

Fig. 9. (a) Solid black line is the mean of the single-binned receiver functions for station COEN and the dashed lines are two standard deviations. The colored lines are the synthetic receiver functions calculated for a 10% velocity dropped over a gradient thickness of 0 to 50 km. b is the same as part a but for station ARMA.

Sp receiver functions at LAB depths is a striking feature of stations in central and western Australia. At cratonic stations near the coast, it is possible that the negative phase found at depths of 69 ± 8 km to 85 ± 14 km, and interpreted to be a MLD, is actually the LAB and that the edge of the thick lithosphere is further inland than resolved by surface wave tomography. However, this explanation is highly unlikely at stations in the continental interior, such as WRAB. It is also possible that the lack of a negative phase at potential LAB depths could reflect the lack of an asthenospheric layer that contains isotropically slow velocities (Gaherty and Jordan, 1995; Pedersen et al., 2009; Revenaugh and Jordan, 1991).

Assuming that an asthenospheric low velocity zone does exist beneath the Australian craton (Cammarano and Romanowicz, 2007; Fishwick et al. (2005); Romanowicz, 2009), modeling with synthetic Sp receiver functions for periods of 10.5 s, comparable to dominant periods in the observed receiver functions, indicates that increasing gradient thickness from 0 km to 50 km produces a 70% reduction in the amplitude of the Sp phase produced by the discontinuity. For velocity drops of no more than 10%, gradient thicknesses of 60 km or more could easily prevent the observation of Sp phases when typical noise levels are taken into account. Sp receiver functions for stations WRAB, FITZ, MBWA and NWAO were re-calculated decreasing the low-pass filter that increased the average dominant period of the individual waveforms from ~10.5 s to ~20 s. Even with these larger dominant periods, no Sp phases from LAB depths were observed. We conclude that if a significant reduction in velocity occurs at the base of the cratonic lithosphere, it must be distributed over 60–90 km or more. Such velocity gradients could be produced by geotherms typical of models where no change in composition or melt content occurs, although comparably gradual vertical variations in composition or melt cannot be ruled out (Fig. 10).

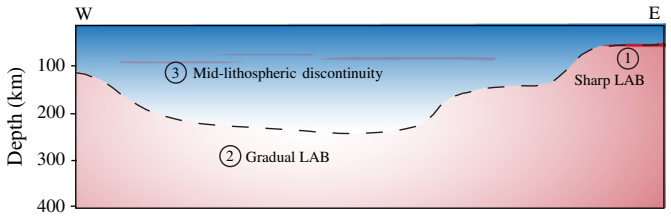

Fig. 10. Schematic cross-section through Australia intersecting Archean, Proterozoic and Phanerozoic terranes. LAB depth estimated from surface wave tomography (Fishwick et al., 2005) and Sp receiver functions (this study).

4.5. A discontinuity within the cratonic lithosphere

The negative Sp phase at 69 ± 8 km to 85 ± 14 km imaged throughout central and western Australia is interpreted to be a negative velocity contrast internal to the lithosphere (a MLD). This feature correlates with a layer of low shear wave velocity in surface wave models, seen in central Australia at 75 km depth by Fishwick et al. (2005), Fishwick and Reading (2008) and more broadly in cratonic Australia by Lekic and Romanowicz (in revision). A decrease in velocity within the cratonic lithosphere at similar depths has also been observed in receiver functions from North America (Abt et al., 2010) and globally in Ps receiver functions (Rychert and Shearer, 2009), surface wave tomography (Romanowicz, 2009) and long-range seismic profiles (Thybo, 2006 and references therein). Discontinuities in the 70–100 km depth range in the continental lithosphere have sometimes been associated with the Hales discontinuity. However, the original definition of this discontinuity was a velocity increase with depth (Hales, 1969), and subsequent citings have included both positive discontinuities (Revenaugh and Jordan, 1991) and anisotropic boundaries (Bostock, 1998; Fuchs, 1983; Levin and Park, 2000; Mercier et al., 2008).

To test whether the negative isotropic velocity gradients associated with MLDs represent averages of an azimuthally anisotropic boundary, the Sp receiver functions were binned in 60° increments as a function of back azimuth. No consistent back-azimuthal patterns in timing or amplitude were observed for the MLD phases (or for LAB Sp phases at eastern Australia stations), although a lack of events in a number of back-azimuth bins hindered the analysis. We conclude that anisotropic layering is not evident, but it cannot be ruled out. Binning by back azimuth was also used to look for variations in Sp phase depth at stations near regions of apparent rapid transitions in LAB depth (e.g. COEN, STKA, and BBOO) inferred from surface wave tomography (Fishwick et al., 2008). However, robust trends in Sp phase depth internal to the data for a single station were not resolved.

Using synthetic Sp receiver function modeling, we determined that a single negative phase similar in amplitude and depth to the observed MLD phases can be produced by isotropic models for the cratonic lithosphere that contain either a thin low velocity layer (<6 km in vertical extent) or a localized drop in velocity (for example a 0 km thick gradient) followed by a gradual increase in velocity of equal magnitude (>50 km thick gradient). Given that aspects of these structures are very localized in depth, they are likely related to factors such as composition or grain size and fabric, rather than vertical variations in temperature. Partial melt could produce sufficiently sharp vertical boundaries, but temperatures estimated for the cratonic lithosphere in Australia (O'Reilly et al., 1997) lie beneath the peridotite solidus, even allowing for the presence of water (Grove et al., 2006).

Layering in composition or texture could date to the formation of the cratonic lithosphere, perhaps related to imbrication of originally thinner lithosphere during mantle accretion. Stacking of lithospheric layers has been suggested in the Canadian shield (Bostock, 1998; Chen, 2009; Mercier et al., 2008; Snyder, 2008), although the discontinuity dips apparent in these studies are not obviously consistent with the relatively uniform depth of the MLD observed in Australia. Another possibility is that the MLD represents the top of a melt cumulate layer (such as a low velocity pyroxenite (Behn and Kelemen, 2006)) emplaced in the cratonic lithosphere during an earlier time when lithospheric temperatures were higher.

5. Conclusions

A strong, coherent negative Sp phase at 61 ± 11 km to 131 ± 9 km in eastern Australia is interpretable as the lithosphere–asthenosphere boundary (LAB). The drop in velocity required to produce the observed phases is too localized in depth (<40 km) to be produced by models in which seismic velocities depend solely on temperature. Rather, the asthenosphere must be made weak relative to the lithosphere by other properties, for example greater water content or a small amount of partial melt. The strongest and shallowest LAB Sp phases correlate with regions of high heat flow and the most recent large volume magmatic eruptions in Australia, suggesting a link between LAB topography and mantle melting processes.

The absence of a negative Sp phase associated with the LAB in cratonic Australia implies that the velocity drop associated with the cratonic LAB is very gradual (distributed over 60–90 km or more) or very weak. Such a gradual boundary could be produced by temperature alone, although gradual variations in mantle composition or melt content cannot be ruled out. The only significant negative Sp phase for stations in central and western Australia is a mid-lithospheric discontinuity found at depths of 69 ± 8 km to 85 ± 14 km. This boundary could represent vertical variations in mantle composition, grain size or fabric, for example a low velocity melt cumulate layer.

Acknowledgements

We thank Scott French for contributions to the analysis and modeling codes, Stewart Fishwick for the Australia shear wave velocity model, Greg Hirth for conversations about interpretation, Rainer Kind for discussion regarding Sp receiver functions, and two anonymous reviewers for their constructive comments. Data were obtained from the IRIS Data Management System. This work was funded by NSF Geophysics award EAR-0538155.

References

Abt, D.L., Fischer, K.M., French, S.W., Ford, H.A., Yuan, H., Romanowicz, B., 2010. North American lithospheric discontinuity structure imaged by Ps and Sp receiver functions. J. Geophys. Res. 115, B09301. doi:10.1029/2009JB006914.

Barley, M.E., Loader, S.E., McNaughton, N.J., 1998. Calc-alkaline volcanism in the McPhee Dome and Kelly Belt, and growth of the eastern Pilbara Craton. Precambr. Res. 88, 3–23.

Behn, M.D., Kelemen, P.B., 2006. Stability of arc lower crust: insights from the Talkeetna arc section, south central Alaska, and the seismic structure of modern arcs. J. Geophys. Res. 111, B11207. doi:10.1029/2006JB004327.

Betts, P.G., Giles, D., Lister, G.S., Frick, L.R., 2002. Evolution of the Australian lithosphere. Aust. J. Earth Sci. 49, 661–695.

Bostock, M.G., 1998. Mantle stratigraphy and evolution of the Slave province. J. Geophys. Res. 103, 21,183–21,200.

Burdick, S., Li, C., Martynov, V., Cox, T., Eakins, J., Mulder, T., Astiz, L., Vernon, F.L., Pavlis, G.L., van der Hilst, R.D., 2008. Upper mantle heterogeneity beneath North America from travel time tomography with global and USArray Transportable Array data. Seis. Res. Lett. 79, 384–392.

Cammarano, F., Romanowicz, B., 2007. Insights into the nature of the transition zone from physically constrained inversion of long-period seismic data. Proc. Natl. Acad. Sci. 104, 9139–9144.

Cawood, P.A., Tyler, I.M., 2004. Assembling and reactivating the Proterozoic Capricorn Orogen: lithotectonic elements, orogenies, and significance. Precambr. Res. 128, 201–218.

Chen, L., 2009. Lithospheric structure variations between the eastern and central North China Craton from S- and P-receiver function migration. Phys. Earth Planet. Int. 173, 216–277.

Chen, L., Zheng, T.Y., Xu, W.W., 2006. A thinned lithospheric image of the Tanlu Fault Zone, eastern China: constructed from wave equation based receiver function migration. J. Geophys. Res. 111, B09312. doi:10.1029/2005JB003974.

Clitheroe, G., Gudmundsson, O., Kennett, B.L.N., 2000a. The crustal thickness of Australia. J. Geophys. Res. 105, 13,697–13,713.
Clitheroe, G., Gudmundsson, O., Kennett, B.L.N., 2000b. Sedimentary and upper crustal structure of Australia from receiver functions. Aust. J. Earth Sci. 47, 209–216.
Collins, J.A., Vernon, F.L., Orcutt, J.A., Stephen, R.A., 2002. Upper mantle structure beneath the Hawaiian swell: constraints from the ocean seismic network pilot experiment. Geophys. Res. Lett. 29, 1522. doi:10.1029/2001GL013302.
Cooper, C.M., Lenardic, A., Moresi, L., 2004. The thermal structure of stable continental lithosphere within a dynamic mantle. Earth Planet. Sci. Lett. 222, 807–817.
Dasgupta, R., Hirschmann, M.M., 2007. Effect of variable carbonate concentration on the solidus of mantle peridotite. Am. Miner. 92, 370–379.
Debayle, E., Kennett, B.L.N., 2000. Anisotropy in the Australasian upper mantle from Love and Rayleigh waveform inversion. Earth Planet. Sci. Lett. 184, 339–351.
Direen, N.G., Crawford, A.J., 2003. The Tasman Line: where is it, and is it Australia's Rodinian breakup boundary? Aust. J. Earth Sci. 50, 491–502.
Ebinger, C.J., Sleep, N.H., 1998. Cenozoic magmatism throughout east Africa resulting from impact of a single plume. Nature 395, 788–791.
Fichtner, A., Kennett, B.L.N., Igel, H., Bunge, H.-P., 2009. Full seismic waveform tomography for upper-mantle structure in the Australasian region using adjoint methods. Geophys. J. Int. 179, 1703–1725.
Fichtner, A., Kennett, B.L.N., Igel, H., Bunge, H.-P., 2010. Full waveform tomography for radially anisotropic structure: new insights into present and past states of the Australasian upper mantle. Earth Planet. Sci. Lett. 290, 270–280.
Fischer, K.M., Ford, H.A., Abt, D.L., Rychert, C.A., 2010. The lithosphere–asthenosphere boundary. Ann. Rev. Earth Planet. Sci. 38, 551–575.
Fishwick, S., Heintz, M., Kennett, B.L.N., Reading, A.M., Yoshizawa, K., 2008. Steps in lithospheric thickness within eastern Australia, evidence from surface wave tomography. Tectonics 27, TC4009. doi:10.1029/2007TC002116.
Fishwick, S., Kennett, B.L.N., Reading, A.M., 2005. Contrasts in lithospheric structure within the Australian craton—insights from surface wave tomography. Earth Planet. Sci. Lett. 231, 163–176.
Fishwick, S., Reading, A.M., 2008. Anomalous lithosphere beneath the Proterozoic of western and central Australia: a record of continental collision and intraplate deformation? Precambrian Res. 166, 111–121.
Fuchs, K., 1983. Recently formed elastic anisotropy and petrological models for the continental subcrustal lithosphere in southern Germany. Phys. Earth Planet. Int. 31, 93–118.
Gaherty, J.B., Jordan, T.H., 1995. Lehmann discontinuity as the base of an anisotropic layer beneath continents. Science 26, 1468–1471.
Gaherty, J.B., Kato, M., Jordan, T.H., 1999. Seismological structure of the upper mantle: a regional comparison of seismic layering. Phys. Earth Planet. Int. 110, 21–41.
Gaul, O.F., Griffin, W.L., O'Reilly, S.Y., Pearson, N.J., 2000. Mapping olivine composition in the lithospheric mantle. Earth Planet. Sci. Lett. 182, 223–235.
Giles, D., Betts, P.G., Lister, G.S., 2001. A continental backarc setting for Early to Middle Proterozoic basins of north-eastern Australia. Geol. Soc. Aust. Abstr. 64, 55–56.
Grove, T.L., Chatterjee, N., Parman, S.W., Médard, E., 2006. The influence of H_2O on mantle wedge melting. Earth Planet. Sci. Lett. 249, 74–89.
Gunn, P.J., Milligan, P., Mackey, T., Liu, S., Murray, A., Maidment, D., Haren, R., 1997. Geophysical mapping using the national airborne and gravity datasets; an example focusing on Broken Hill. J. Aust. Geol. Geophys. 17, 127–136.
Hales, A.L., 1969. A seismic discontinuity in the lithosphere. Earth Planet. Sci. Lett. 7, 44–46.
Hammond, W.C., Humphreys, E.D., 2000. Upper mantle seismic wave velocity: effects of realistic partial melt geometries. J. Geophys. Res. 105, 10,975–10,986.
Hansen, S.E., Nyblade, A.A., Julià, J., Dirks, P.H.G.M., Durrheim, R.J., 2009. Upper-mantle low-velocity zone structure beneath the Kaapval craton from S-wave receiver functions. Geophys. J. Int. 178, 1021–1027.
Hansen, S.E., Rodgers, A.J., Schwartz, S.Y., Al-Amri, A.M.S., 2007. Imaging ruptured lithosphere beneath the Red Sea and Arabian Peninsula. Earth Planet. Sci. Lett. 259, 256–265.
Heit, B., Sodoudi, F., Yuan, X., Bianchi, M., Kind, R., 2007. An S receiver function analysis of the lithospheric structure in South America. Geophys. Res. Lett. 34, L14307. doi:10.1029/2007GL030317.
Hill, D., 1951. Geology. In: Mack, G. (Ed.), Handbook of Queensland. Australian Association for the Advancement of Science, Brisbane.
Hirschmann, M.M., Tenner, T., Aubaud, C., Withers, A.C., 2009. Dehydration melting of nominally anhydrous mantle: the primacy of partitioning. Phys. Earth Planet. Int. 176, 54–68.
Hirth, G., Kohlstedt, D.L., 1996. Water in the oceanic upper mantle: implications for rheology, melt extraction and the evolution of the lithosphere. Earth Planet. Sci. Lett. 144, 93–108.
Johnson, R.W., Knutson, J., Taylor, S.R., 1989. Intraplate Volcanism in Eastern Australia and New Zealand. Cambridge University Press, Melbourne.
Kaiho, Y., Kennett, B.L.N., 2000. Three-dimensional seismic structure beneath the Australasian region from refracted wave observations. Geophys. J. Int. 142, 651–668.
Karato, S., Jung, H., 1998. Water, partial melting and the origin of the seismic low velocity and high attenuation zone in the upper mantle. Earth Planet. Sci. Lett. 157, 193–207.
Kawakatsu, H., Kumar, P., Takei, Y., Shinohara, M., Kanazawa, T., Araki, E., Suyehiro, K., 2009. Seismic evidence for sharp lithosphere–asthenosphere boundaries of oceanic plates. Science 324, 499–502.
Keith, C.M., Crampin, S., 1977. Seismic body waves in anisotropic media: synthetic seismograms. Geophys. J. R. Astron. Soc. 49, 225–243.
Kennett, B.L.N., 1991. The removal of free surface interactions from three-component seismograms. Geophys. J. Int. 104, 153–163.
Kennett, B.L.N., Engdahl, E.R., Buland, R., 1995. Constraints on seismic velocities in the Earth from travel-times. Geophys. J. Int. 122, 108–124.
Kikuchi, M., Kanamori, H., 1982. Inversion of complex body waves. Bull. Seismol. Soc. Am. 72, 491–506.
King, S.D., Ritsema, J., 2000. African hot spot volcanism: small-scale convection in the upper mantle beneath cratons. Science 290, 1137–1140.
Korenaga, J., Jordan, T.H., 2002. On the state of sublithospheric upper mantle beneath a supercontinent. Geophys. J. Int. 149, 179–189.
Kumar, P., Kind, R., Hanka, W., Wylegalla, K., Reigber, C., Yuan, X., Woelbern, I., Schwintzer, P., Fleming, K., Dahl-Jensen, T., Larsen, T.B., Schweitzer, J., Priestley, K., Gudmundsson, O., Wolf, D., 2005b. The lithosphere–asthenosphere boundary in the North-West Atlantic region. Earth Planet. Sci. Lett. 236, 249–257.
Kumar, P., Yuan, X., Kind, R., Kosarev, G., 2005a. The lithosphere–asthenosphere boundary in the Tien Shan-Karakoram region from S receiver functions: evidence for continental subduction. Geophys. Res. Lett. 32, L07305. doi:10.1029/2004GL022291.
Kumar, P., Yuan, X.H., Kumar, M.R., Kind, R., Li, X.Q., Chadha, R.K., 2007. The rapid drift of the Indian tectonic plate. Nature 449, 894–897.
Lee, C.T.A., 2003. Compositional variation of density and seismic velocities in natural peridotites at STP conditions: implications for seismic imaging of compositional heterogeneities in the upper mantle. J. Geophys. Res. 108. doi:10.1029/2003JB002413.
Lekic, V., Romanowicz, B., in revision. Inferring upper mantle structure by full waveform tomography with the Spectral Element Method. Geophys. J. Int.
Levin, V., Park, J., 2000. Shear zones in the Proterozoic lithosphere of the Arabian Shield and the nature of the Hales discontinuity. Tectonophysics 323, 131–148.
Li, X., Kind, R., Priestley, K., Sobolev, S.V., Tilmann, F., Yuan, X., Weber, M., 2000. Mapping the Hawaiian plume conduit with converted seismic waves. Nature 405, 938–941.
Li, X., Kind, R., Yuan, X.H., Wolbern, I., Hanka, W., 2004. Rejuvenation of the lithosphere by the Hawaiian plume. Nature 427, 827–829.
Li, X., Yuan, X., Kind, R., 2007. The lithosphere–asthenosphere boundary beneath the western United States. Geophys. J. Int. 170, 700–710.
Ligorria, J.P., Ammon, C.J., 1999. Iterative deconvolution and receiver-function estimation. Bull. Seismol. Soc. Am. 89, 1395–1400.
Mercier, J.-P., Bostock, M.G., Audet, P., Gaherty, J.B., Garnero, E.J., Revenaugh, J., 2008. The teleseismic signature of fossil subduction: Northwestern Canada. J. Geophys. Res. 113, B04308. doi:10.1029/2007JB005127.
Mohsen, A., Kind, R., Sobolev, S.V., Weber, M., Group, D.E.S.E.R.T., 2006. Thickness of the lithosphere east of the Dead Sea Transform. Geophys. J. Int. 167, 845–852.
Nettles, M., Dziewonski, A.M., 2008. Radially anisotropic shear velocity structure of the upper mantle globally and beneath North America. J. Geophys. Res. 113, 61–67.
O'Reilly, S.Y., Griffin, W.L., Gaul, O., 1997. Paleogeothermal gradient in Australia: key to 4-D lithosphere mapping. J. Aust. Geol. Geophys. 17, 63–72.
Oreshin, S., Vinnik, L., Peregoudov, D., Roecker, S., 2002. Lithosphere and asthenosphere of the Tien Shan imaged by S receiver functions. Geophys. Res. Lett. 29, 1191. doi:10.1029/2001GL014441.
Ozacar, A.A., Gilbert, H., Zandt, G., 2008. Upper mantle discontinuity structure beneath East Anatolian Plateau (Turkey) from receiver functions. Earth Planet. Sci. Lett. 269, 426–434.
Pedersen, H.A., Fishwick, S., Snyder, D.B., 2009. A comparison of cratonic roots through consistent analysis of seismic surface waves. Lithos 109, 81–95.
Reading, A.M., Kennett, B.L.N., 2003. Lithospheric structure of the Pilbara Craton, Capricorn Orogen and northern Yilgarn Craton, Western Australia, from teleseismic receiver functions. Aust. J. Earth Sci. 50, 439–445.
Reading, A.M., Kennett, B.L.N., Dentith, M.C., 2003. Seismic structure of the Yilgarn Craton, Western Australia. Aust. J. Earth Sci. 50, 427–438.
Reading, A.M., Kennett, B.L.N., Goleby, B., 2007. New constraints on the seismic structure of West Australia: evidence for terrane stabilization prior to the assembly of an ancient continent? Geology 35, 379–382.
Revenaugh, J.S., Jordan, T.H., 1991. Mantle layering from ScS reverberations: 3. The upper mantle. J. Geophys. Res. 96, 19,781–19,810.
Romanowicz, B., 2009. The thickness of tectonic plates. Science 324, 474–476.
Rychert, C.A., Fischer, K.M., Rondenay, S., 2005. A sharp lithosphere–asthenosphere boundary imaged beneath eastern North America. Nature 436, 542–545.
Rychert, C.A., Rondenay, S., Fischer, K.M., 2007. P-to-S and S-to-P imaging of a sharp lithosphere–asthenosphere boundary beneath eastern North America. J. Geophys. Res. 112, B08314. doi:10.1029/2006JB004619.
Rychert, C.A., Shearer, P.M., 2009. A global view of the lithosphere–asthenosphere boundary. Science 324, 495–498.
Rychert, C.A., Shearer, P.M., Fischer, K.M., 2010. Scattered Wave Imaging of the Lithosphere–Asthenosphere Boundary. Lithos 120, 173–185.
Sacks, I.S., Snoke, J.A., Husebye, E.S., 1979. Lithosphere thickness beneath the Baltic shield. Tectonophysics 56, 101–110.
Simons, F.J., van der Hilst, R.D., 2002. Age-dependent seismic thickness and mechanical strength of the Australian lithosphere. Geophys. Res. Lett. 29, 1529–1533.
Simons, F.J., van der Hilst, R.D., 2003. Seismic and mechanical anisotropy and the past and present deformation of the Australian lithosphere. Earth Planet. Sci. Lett. 211, 271–286.
Simons, F.J., Zielhuis, A., van der Hilst, R.D., 1999. The deep structure of the Australian continent from surface-wave tomography. Lithos 48, 17–43.
Snyder, D.B., 2008. Stacked uppermost mantle layers within the Slave craton of NW Canada as defined by anisotropic seismic discontinuities. Tectonics 27, TC4006. doi:10.1029/2007TC002132.
Sodoudi, F., Yuan, X., Liu, Q., Kind, R., Chen, J., 2006. Lithospheric thickness beneath the Dabie Shan, central eastern China from S receiver functions. Geophys. J. Int. 166, 1363–1367.

Takei, Y., 2002. Effect of pore geometry of Vp/Vs: from equilibrium geometry to crack. J. Geophys. Res. 107, B22043. doi:10.1029/2001JB005850.
Takei, Y., Holtzman, B.K., 2009. Viscous constitutive relations of solid–liquid composites in terms of grain boundary contiguity: 1. Grain boundary diffusion control model. J. Geophys. Res. 114, B06205. doi:10.1029/2004JB002965.
Thybo, H., 2006. The heterogeneous upper mantle low velocity zone. Tectonophysics 416, 53–79.
Tyler, I.M., 2001. Collisional orogeny during the Paleoproterozoic in Western Australia. Geol. Soc. Aust. Abstr. 64, 187–188.
Vinnik, L., Kurnik, E., Farra, V., 2005. Lehmann discontinuity beneath North America: no role for seismic anisotropy. Geophys. Res. Lett. 32, L09306. doi:10.1029/2004GL022333.
Wellman, P., 1983. Hotspot volcanism in Australia and New Zealand: Cainozoic and mid-Mesozoic. Tectonophysics 96, 225–243.
Wellman, P., 1998. Mapping of geophysical domains in the Australian continental crust using gravity and magnetic anomalies. In: Braun, J., Dooley, J., Goleby, B., van der Hilst, R., Klootwijk, C. (Eds.), Structure and Evolution of the Australian Continent: American Geophysical Union Geodynamics Series, 26, pp. 59–71.
Wellman, P., McDougall, I., 1974. Cainozoic igneous activity in eastern Australia. Tectonophysics 23, 49–65.
Wilson, D., Grand, S., Angus, D., Ni, J., 2006. Constraints on the interpretation of S-to-P receiver functions. Geophys. J. Int. 165, 969–980.
Wittlinger, G., Farra, V., 2007. Converted waves reveal a thick and layered tectosphere beneath the Kalahari super craton. Earth Planet. Sci. Lett. 254, 404–415.
Wolbern, I., Jacob, A.W.B., Blake, T.A., Kind, R., Li, X., Yuan, S., Duennebier, F., Weber, M., 2006. Deep origin of the Hawaiian tilted plume conduit derived from receiver functions. Geophys. J. Int. 166, 767–781.
Yuan, H., Romanowicz, B., 2010. Lithospheric layering in the North American Craton. Nature 466, 1063–1068.
Yuan, X., Kind, R., Li, X., Wang, R., 2006. The S receiver functions: synthetics and data example. Geophys. J. Int. 165, 555–564.
Zhu, L., Kanamori, H., 2000. Moho depth variation in southern California from teleseismic receiver functions. J. Geophys. Res. 105, 2969–2980.